Investigation of effective-medium models of microscopic surface roughness by spectroscopic ellipsometry

D. E. Aspnes and J. B. Theeten*

Bell Laboratories, Murray Hill, New Jersey 07974

F. Hottier

Laboratoires d'Electronique et de Physique, 94450 Limeil-Brevannes, France
(Received 9 March 1979)

Using measured dielectric function data from 2.1 to 5.5 eV for chemical-vapor-deposition—grown smooth amorphous (a-Si) and microscopically rough fine-grained polycrystalline (p-Si) films, we show that the dielectric properties of microscopically rough layers of thicknesses 100–500 Å are accurately modeled in the effective-medium approximation. These microscopically rough layers show essentially no macroscopic light scattering, and thus are inaccessible to measurement by usual scattering techniques. The unambiguous identification of microscopic roughness, as opposed to, e.g., an overlying oxide, is shown to require a spectroscopic capability. Statistical-analysis techniques are introduced to determine model parameters systematically and objectively, and also to establish correlations and confidence limits that show which parameters are defined by the data and which are statistically indeterminate. A best-fit five-parameter model for the sample with the thickest surface region shows that the density profile is characteristic of hemispherical, not pyramidal, irregularities. This indicates that surface roughness arises from a three-dimensional nucleation and growth process in these samples. In a comparison of the three one-parameter effective-medium models, Bruggeman and Maxwell Garnett(2) theories are found to adequately represent the data, while the Lorentz-Lorenz model, previously used exclusively to model roughness in single-wavelength applications, predicts only qualitatively the spectral dependence and gives poor results.

I. INTRODUCTION

One factor that can influence significantly the measured dielectric properties of "real" materials, particularly as determined by ellipsometry, is surface roughness.[1-21] Roughness can be characterized approximately by a mean height of irregularities about an average plane, and a correlation length between irregularities.[22] Roughness is clearly a relative quantity, depending upon the ratio of the length scale of the irregularities to the wavelength of light. The surface is macroscopically rough and scatters light if the length scale of the irregularities is of the order of or exceeds the wavelength of light.

We are concerned here with microscopic roughness, where the mean height and correlation length of the irregularities are both much less than the wavelength of light. Under these restrictions, multiple-scattering depolarization is not significant and the contribution of the field-induced polarization of the rough surface to the far-field radiation pattern measured experimentally can be approximated[23,24] by one or more layers of a polarizable effective medium that is sandwiched between a perfect substrate and a perfect ambient. This model has been invoked rather extensively in ellipsometric measurements at a single

wavelength,[2-11] and related numerical computations[4,5,9,10,12-15] based on the Lorentz-Lorenz effective-medium theory.

Unfortunately, a number of phenomena, such as oxide overlayers or the unintentional modification of the substrate dielectric properties by damage from mechanical polishing, can simulate the effect of roughness.[7,8] In essence, it is not possible to detect roughness unambiguously from single-wavelength ellipsometric data, where only two parameters are available. Here, the parameters of any roughness model are highly underdetermined, even though some additional information can be obtained by varying the angle of incidence. For this reason, we do not believe that the effective-medium model of microscopic roughness has yet been tested adequately. We shall show, in fact, that the Lorentz-Lorenz model, which has been used exclusively to date in this application, is a poor choice and that the Bruggeman self-consistent model is significantly better.

The development of fast, automatic, spectroscopic ellipsometers[25-29] that can measure the complex reflectance ratio quickly and accurately has made a spectral test of effective-medium modeling of microscopic roughness possible. Moreover, recent interest in using ellipsometry to characterize surface quali-

ty[7,8,16,21] or nucleation, quality, and growth of chemical-vapor-deposited (CVD) and plasma-deposited thin films[11,30,31] or porous or partially annealed heterogeneous solids[32] makes such a comparison relevant.

In this paper we investigate effective-medium descriptions of roughness over an extended spectral range, 2.1−5.5 eV, on CVD amorphous (a-Si) or fine-grained polycrystalline (p-Si) films of different roughnesses. We chose these materials for the investigation because their dielectric properties change from dielectriclike to metallic as the wavelength is decreased. This leads to qualitatively different constraints on any effective-medium model of surface roughness without changing surfaces, and thus insures a legitimate test of effective-medium representations. Also, the dielectric function of these materials does not have sharp structure that may be influenced by extrinsic effects such as grain size or internal stress. Moreover, samples of various degrees of roughness may be produced by controlling substrate temperature and ambient stoichiometry and pressure conditions.

The outline of the paper is as follows. Experimental details are summarized in Sec. II. A brief discussion of one-parameter effective-medium models is given in Sec. III A, and a description of the approach leading to best-fit parameters is outlined in Sec. III B. The dielectric function of a-Si from 1.5 to 5.8 eV is reported in Sec. IV A and compared to previous data for this material.[33,34]

In Secs. IV B and IV C, we compute best-fit parameters for roughness models of increasing complexity for two samples showing moderate and substantial microscopic roughnesses, respectively. The results show that the Bruggeman effective-medium approximation gives a good representation of the data over the entire accessible spectral region for both samples, a nontrivial result that demonstrates the general validity of an effective-medium description for microscopic roughness. The approximate density profile is obtained by a two-layer fit to the sample with the thickest surface region. This profile is compared to several model profiles in Sec. IV D to show that it is incompatible with pyramid or ridge models previously proposed to describe roughness in other systems, but instead agrees well with a model based on hemispherical bumps. This is expected if a three-dimensional nucleation process is responsible for film growth and consequent roughness in this material.

Finally, we compare in Sec. IV E the predictions of the Lorentz-Lorenz, Maxwell Garnett, and Bruggeman effective-medium models and show that the Maxwell Garnett(2) and the Bruggeman models give good fits, with the Bruggeman model slightly favored on experimental and clearly favored on physical grounds. The Lorentz-Lorenz approximation, which has been used exclusively in previous rough-surface

modeling calculations,[4,5,9,10,12−15] gives poor results and reproduces the spectral behavior of the data only qualitatively. All results emphasize the necessity of spectral measurements to determine the properties of the rough surface.

II. EXPERIMENTAL

The Si films investigated here were deposited by pyrolysis of SiH_4 diluted in H_2 in a low-pressure (typically 10 Torr) chamber. The substrates were (111) Si wafers that were covered with 3500 Å of silicon nitride. Table I summarizes the various growth conditions for the three typical samples analyzed in Sec. IV. From previous published work[35−38] as well as transmission-electron-microscopy (TEM) and reflection high-energy electron diffraction (RHEED) examinations of our sample, we determined that the Si films deposited at low temperature (under 560 °C) were totally amorphous. Above a critical temperature, the material becomes polycrystalline. The grain size is increased when the temperature is increased, and, to a lesser extent, when the pressure and the rate of growth are decreased. For the conditions given in Table I, the RHEED patterns were featureless (575 °C) or consisted of continuous diffuse rings (740 and 870 °C) indicative of a very small grain size (below 100 Å) together with a random orientation of the grains.

The presence of microscopic roughness was verified by TEM measurements of replica films. The replicas were shadowed by Pt evaporated at 45 ° angle of incidence. The TEM picture is shown in Fig. 1 for the T =870 °C sample. The surface is seen to be irregular, having a random texture with features separated by distances of the order of 500−1000 Å. The well-defined shadowing apparent in Fig. 1 shows that the height distribution is somewhat less, but of the order of, the feature separation. As expected, the TEM replicas indicated that the scale of rough-

TABLE I. Deposition conditions for the three samples used in this experiment.

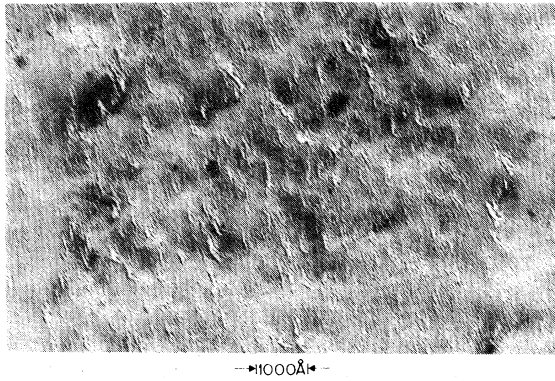| Type of sample	Deposition temperature (°C)	Deposition pressure (Torr)	Thickness of deposit (Å)	Rate of growth (Å/m)
Smooth	575	10	5000	100
Moderately rough	740	10	5000	1000
Rough	870	350	7500	1500

FIG. 1. TEM micrograph of Pt-shadowed replica of the surface of the roughest sample investigated here. Magnification is indicated in figure.

ness is related to, but larger than, the grain size. The samples accordingly can be represented as smooth ($T = 575$ °C), moderately rough ($T = 740$ °C), or rough ($T = 870$ °C), as indicated in Table I.

The samples were checked for macroscopic roughness by light scattering. Intensity versus scattering angle data for 6328-Å s-polarized light incident at 70° are shown in Fig. 2 for the three samples studied in this work, together with the instrument resolution curve. As can be seen, in all cases the scattered light essentially follows the instrument limit to 10^{-6} in the ratio of the scattered intensity, I_s, to the specularly
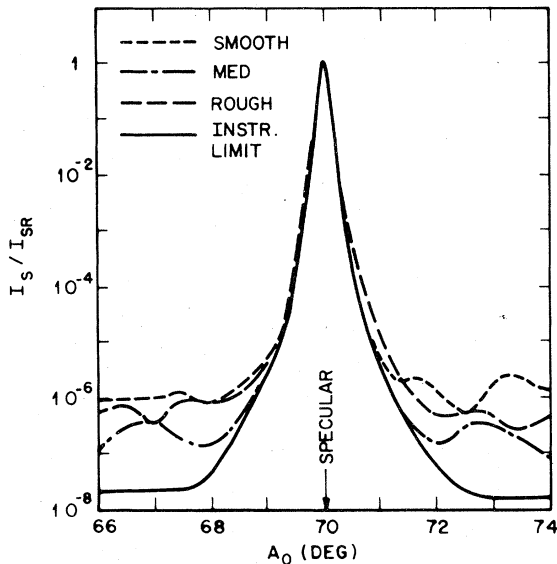

FIG. 2. Scattering intensities as a function of observation angle for the three samples investigated here, compared to instrument resolution.

reflected intensity, I_{sr}. The oscillations in the wings arise from multiple interference within the film. In the Rayleigh-Fano theory[39] the 10^{-6} scattering intensities in our scattering geometry (1-mm incident beam diameter, solid angle corresponding to 1-mm aperture 40 cm from light spot) correspond to statistical roughness parameters (amplitudes of surface Fourier coefficients $|\rho_G|$) of the order of 2 Å. Thus the assumption of negligible *macroscopic* roughness seems to be satisfied very well for these samples. The absence of macroscopic scattering shows that microscopic roughness is not detected by usual light-scattering techniques. The microscopically rough samples may have large effective surface areas and thus have obvious implications in the magnitudes of apparent surface Raman scattering intensities, although this point was not investigated here.

Data were taken using an automatic spectroscopic rotating-analyzer ellipsometer described in detail elsewhere.[28] All measurements were performed in a dry N_2 atmosphere after cleaning the surfaces *in situ* with methanol to reduce any influence from surface contamination. A 2-mm aperture was used 1 cm from the sample to define accurately the measured area, which was the projected image of this aperture at an angle of incidence of 67.08°. The resulting data were corrected for optical activity in the quartz Rochon prisms as discussed previously.[40]

III. THEORY

A. Effective-medium models

The Lorentz-Lorenz (LL), Maxwell Garnett (MG) and Bruggeman effective-medium approximation (EMA) models are simple effective-medium theories[41,42] that represent a heterogeneous dielectric mixture by a single parameter. Therefore, they represent a natural first approximation to model a rough surface layer. Because their differences have not been appreciated in previous rough-surface applications we briefly discuss their qualitative similarity and quantitative differences. These differences are substantial if the dielectric functions of the components of a heterogeneous mixture are themselves substantially different, as is the case for voids in semiconductors or metals.

The LL, MG, and EMA models all have the same generic form

$$\frac{\langle \epsilon \rangle - \epsilon_h}{\langle \epsilon \rangle + 2\epsilon_h} = v_1 \frac{\epsilon_1 - \epsilon_h}{\epsilon_1 + 2\epsilon_h} + v_2 \frac{\epsilon_2 - \epsilon_h}{\epsilon_2 + 2\epsilon_h} + \cdots \quad , \quad (1)$$

where $\langle \epsilon \rangle$, ϵ_h, $\epsilon_1, \epsilon_2, \ldots$, are the (complex) dielectric functions of the effective medium, host medium, and inclusions of types $1, 2, \ldots$, in the host, respectively, and where $v_1, v_2, \ldots$, represent volume fractions

of material of types $1, 2, \ldots$, in the total volume.
The underlying assumptions are (i) spherical inclu-
sion geometry, and (ii) dipole interactions only.[42,43]
Neither assumption is rigorously satisfied by a rough
layer, but in the absence of resonances the modifica-
tions resulting from changing the depolarization fac-
tors from the spherical value of $\frac{1}{3}$ are not generally
significant, and the dipole interaction is a standard
first approximation that appears to give good results
in bulk systems.[43] We note that intrinsic anisotropy
appropriate to monolayers is not expected to apply to
roughness layers beyond a few Å in thickness, con-
trary to previous assumptions,[14] because Ewald sums
attain 96% of their value in a single atomic plane.[23]

In the LL approximation, which was developed to
describe point polarizable entities of polarizability α
embedded in vacuum, $\epsilon_h = 1$ and the volume frac-
tions are evaluated directly from the number, N_i, of
atoms/molecules of each species present and the
volume n_i^{-1} per atom/molecule, where n_i is the
number density per unit volume. Thus

$$v_i = N_i n_i^{-1} / \sum_j N_j n_j^{-1} , \qquad (2)$$

whence $\sum_L v_i = 1$. Although not used here, the LL
relation is usually expressed in terms of the polariza-
bilities α_i, which are related to the macroscopic
dielectric function ϵ_i of the homogeneous phase i by
the Clausius-Mossotti relation

$$\frac{4}{3} \pi n_i \alpha_i = \frac{\epsilon_i - 1}{\epsilon_i + 2} . \qquad (3)$$

The MG approximation[44] corresponds to macro-
scopic dielectric inclusions in a host dielectric back-

ground and in this case the quantities in Eq. (1) have
their obvious interpretations. Because inclusions can
occupy any volume fraction up to unity $\sum_j v_j \lesssim 1$.
What has not been appreciated in rough-surface ap-
plications, however, is that for a single type of inclu-
sion in a host background $\langle \epsilon \rangle$ has different values in
the MG theory if the role of host and inclusion is
interchanged—even if the respective volume fractions
are held constant.[42] To avoid this ambiguity in bulk
applications Bruggeman[45] suggested replacing ϵ_h in
Eq. (1) with $\langle \epsilon \rangle$, i.e., letting the effective medium it-
self act as host medium. Thus, self-consistency is
achieved and $\sum_i v_i = 1$. The above discussion should
make clear that, despite apparent wide differences in
models or final mathematical form, the LL, MG, and
EMA formulations reduce simply to different choices
for the host material dielectric function, ϵ_H.

Nevertheless, if the host-inclusion dielectric func-
tions differ by an order of magnitude, as is the typical
case for voids in semiconductors and metals, the
differences in $\langle \epsilon \rangle$ among the three models are sub-
stantial. We illustrate this point in Fig. 3 with regard
to a hypothetical medium of 50% voids and 50% a-Si,
using a-Si data to be discussed. For simplicity only
the imaginary part of $\langle \epsilon \rangle$ is shown. As explained
above, the LL and MG(1) (where the a-Si is as-
sumed to be embedded in the void) models give
identical results. Figure 3 shows that these results
are very different from the MG(2) model, where
voids are assumed to be embedded in a-Si, despite
the fact that the relative volume fractions are identi-
cal. [The MG(1) and MG(2) models differ only in
the choice of host material.] The EMA calculation
falls between MG(1) and MG(2), a rigorous result of
self-consistency that can be shown to be valid under
fairly general conditions.[46] The standard LL or
MG(1) model grossly underestimates the effect of
the absorptive component relative to EMA and
MG(2).

To choose the correct effective-medium model to
use—for either bulk or rough surface applications—is
in fact more important than to consider details of
possible surface anisotropy, as a comparison between
Fig. 3 and the results of Ref. 14 will demonstrate.
Unfortunately, even in the simpler bulk case the
question of which model (if any) is best is far from
settled. Conductivity measurements on bulk sys-
tems[47] appear to favor the EMA. Optical transmis-
sion data[48] on thin ($\sim$400 Å) Ag-SiO$_2$ cermet films
have been interpreted[49] as favoring the MG model.
But these data show characteristics of EMA as well,
and the MG conclusion has recently been ques-
tioned.[50] Because rough surfaces consist of effective
mixtures ranging from mostly a-Si to mostly void, we
shall use the EMA which treats these constituents on
an equal basis and is therefore physically more ap-
pealing. Our data in fact favor the EMA and the
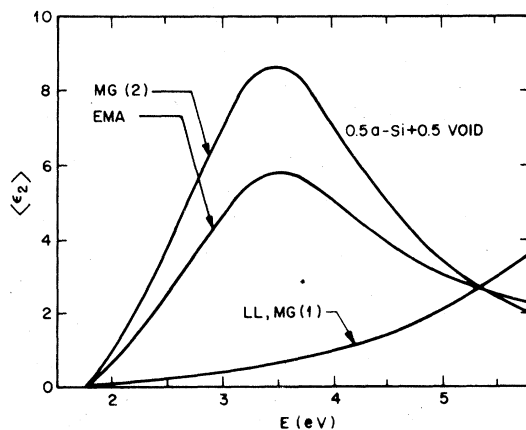point will be discussed more fully in Sec. IV A.

FIG. 3. Comparison of imaginary parts $\langle \epsilon_2 \rangle$ of effective
dielectric functions for a 50% a-Si, 50% void mixture as cal-
culated by the LL, MG(1), EMA, and MG(2) models.

B. Best-fit determination

The ellipsometric data consist of $\tan\Psi$, $\cos\Delta$ spectra, in principle from 1.5 to 5.8 eV. Due to multiple internal reflections in regions of transparency the useful spectral range for all films measured here lay above 2.1 eV. For comparison with model calculations, these data were converted to the complex reflectance ratio $\rho = \tan\Psi[\cos\Delta - i(1-\cos^2\Delta)^{1/2}]$.

Model calculations of ρ were performed assuming a multilayer configuration on a uniform substrate using standard equations.[20] All layers, including the substrate, were assumed to consist of EMA mixtures of the measured dielectric function of a-Si, obtained from the $T = 575\,^\circ$C sample, and voids. The presence of voids in the $T = 740$ and $870\,^\circ$C p-Si samples was confirmed by TEM micrographs of back-thinned samples. In principle, a difficulty can arise if the a-Si data are used to describe the p-Si samples. For example in a previous investigation of p-Si films grown on spinel, a dielectric function midway between those of a-Si and c-Si was reported.[51] Even if such an error were present in our data, dielectriclike and metallic behavior would still occur in the same spectral regions, and the large phase changes observed in ρ relative to smooth-surface model calculations could not be explained except by overlayers. The excellent fits to be discussed appear to justify the assumption that all our samples have the same dielectric function. Significant differences could occur if the grain sizes were bigger and not randomly oriented, as may be the case for films deposited on spinel[51] instead of amorphous Si_3N_4 as used here.

Rough-surface overlayers were modeled by thickness and by void fraction within the EMA, as discussed above. For some calculations the outermost layer was taken to be SiO_2 for comparison purposes. The dielectric function for SiO_2 was taken from the literature.[52] Thus, the variable parameters in the model calculations, i.e., the number of layers, type of outer layer, void concentrations, and layer thicknesses, are all energy independent.

Calculated and experimental values of ρ were compared systematically, objectively, and quantitatively by evaluating the mean-square deviation

$$\delta = \left[\frac{1}{N-1} \sum_{i=1}^{N} |\rho_{\text{calc}}(E_i) - \rho_{\text{exp}}(E_i)|^2 \right]^{1/2}, \quad (4)$$

where N is the number of points equally spaced in energy over the spectral range. For a given configuration the model parameters were determined by minimizing δ by standard least-squares linear regression analysis techniques,[53] which were also used to calculate $\hat{\sigma}$, the unbiased estimator of δ, and the 90% confidence limits of the best-fit parameters. The "quality" of a given model can be inferred from its value of $\hat{\sigma}$. Parameters within a given model that are

well defined by the data will have low 90% confidence limits. Confidence limits also prevent irrelevant or excessive use of parameters, as the limits increase catastrophically under these conditions.

IV. RESULTS AND DISCUSSION

A. Dielectric function of a-Si

The dielectric function data for the $T = 575\,^\circ$C a-Si film are shown in Fig. 4. The influence of any SiO_2 overlayer would be to lower the maximum of ϵ_2. To investigate this, we compared our results to the a-Si data of Pierce and Spicer,[34] obtained from a Kramers-Kronig transformation of reflectance measurements on samples prepared and measured in ultrahigh vacuum. The agreement in peak heights is excellent, showing the SiO_2 overlayer to be negligible. The overall agreement is very good, with maximum differences of the order of 8% over the energy range for which a comparison is possible. This difference is due primarily to the CVD material having an absorption edge slightly higher in energy, probably as a result of hydrogen incorporated during the CVD process. Slightly larger differences, of the order of 10%, are observed with respect to the data of Philipp,[33] where the ϵ_2 maximum is notably smaller.

Because of the interference by multiple internal reflections within the CVD film, our data terminate at 2.5 eV. At lower energies we use the dashed-line extrapolation of Pierce-Spicer data. Our data with the Pierce-Spicer extrapolation were used to calculate Fig. 3.
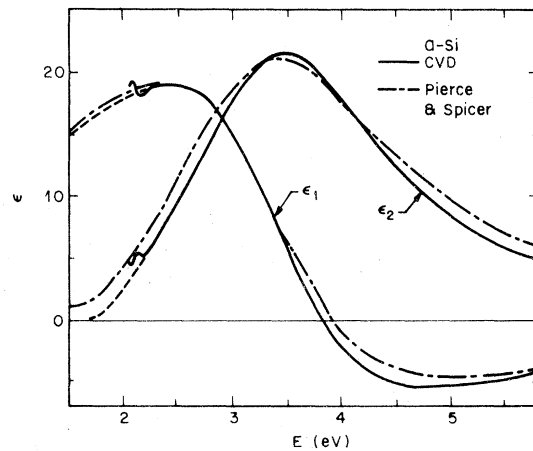

FIG. 4. Dielectric function of a-Si (———) measured on smooth CVD sample; (———————) after Ref. 34. Dashed line shows extrapolation through region of interference oscillations.

B. Moderately rough sample

Model calculation parameters of increasingly better fit for the moderately rough sample are shown in Fig. 5. Also shown are the respective values of $\hat{\sigma}$, beginning with a bare a-Si substrate (no attempt to simulate roughness or to include voids) and ending with a three-parameter model with voids present not only in the single overlayer but also in the uniform substrate. The best-fit parameters are shown in the schematic below, and summarized with their 90% confidence limits in Table II. The models are ranked in order of increasingly better fit. For these computations, 71 points were used over an energy range of 2.1 to 5.8 eV.

To provide some feeling for the meaning of agreement between calculation and experiment, we compare in Fig. 6 the $\tan\Psi$, $\cos\Delta$ spectra actually measured by the rotating-analyzer ellipsometer to calculated $\tan\Psi$, $\cos\Delta$ spectra for the one-parameter SiO_2 and three-parameter models of Fig. 5. These have $\hat{\sigma}$ values of 0.098 and 0.018, respectively.

Figure 5 shows that the assumption of a single SiO_2 layer on an a-Si substrate does not provide a good fit even with an unrealistically large oxide thickness of 67 Å. Figure 6 shows why. The thickness variable is used to adjust the phase, Δ, of the model calculation to give a reasonably good approximation to the mea-

TABLE II. Best-fit parameters and their 90% confidence limits for the moderately rough sample (see Fig. 5), listed in increasing goodness of fit.

Substrate	First layer	$\hat{\sigma}$
a-Si	$\cdots$	0.18
a-Si	SiO_2, $d = 67 \pm 9$ Å	0.098
a-Si + void $(29 \pm 1\%)$	$\cdots$	0.047
a-Si	a-Si + void $(31 \pm 1\%)$, $d = 166 \pm 15$ Å	0.035
a-Si + void $(25 \pm 1\%)$	SiO_2, $d = 24 \pm 4$ Å	0.030
a-Si + void $(19 \pm 1\%)$	a-Si + void $(44 \pm 6\%)$, $d = 53 \pm 16$ Å	0.018

sured phase spectrum, but the model amplitude spectrum $\tan\Psi = |\rho|$ cannot be brought into agreement with the measured amplitude spectrum because the dielectric function of SiO_2 is too low. Thus a single oxide layer on an a-Si substrate cannot explain adequately the data.

By allowing the uniform substrate to contain voids, thus reducing the average impedance mismatch between ambient and substrate, the amplitude is adjusted without significantly affecting the phase and much better agreement is obtained. Substantial further improvements follow by increasing the complexity of the models as shown in Fig. 5 and Table II. The fact that in every case models with an effective-medium overlayer fit the data significantly better than equivalent models with an SiO_2 overlayer shows
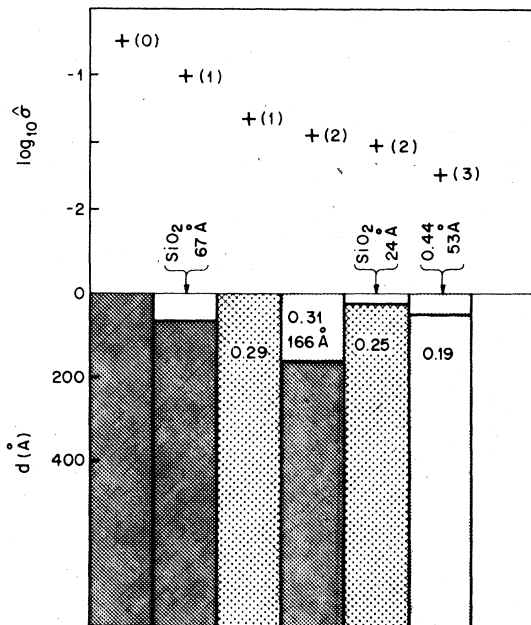

FIG. 5. Schematic of models of increasing complexity obtained by best-fit comparisons of calculated values of ρ to moderately-rough-sample data. Values of $\hat{\sigma}$ are plotted at top. Numbers in lower bars, if given, represent volume fraction of voids in a-Si as calculated in the EMA. Uncertainties are given in Table II.
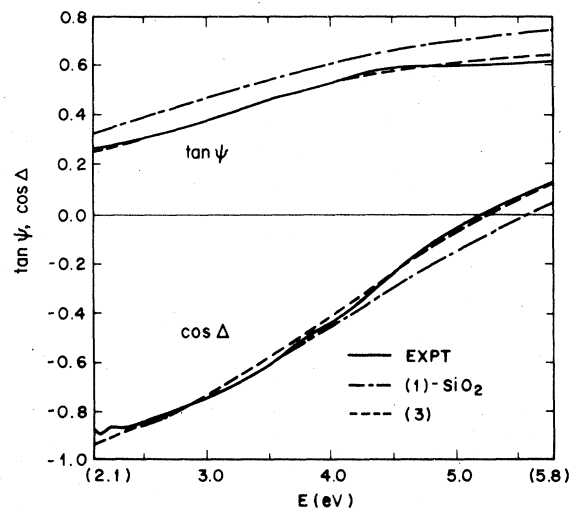

FIG. 6. Comparison between $\tan\Psi$, $\cos\Delta$ data (——) and similar curves calculated for the one-parameter SiO_2 (— · —) and three-parameter (— — —) models of Fig. 5.

that the major contributor to the outer-layer effective dielectric function is roughness. The best fit is also shown in Fig. 6, and is seen to agree very well with experiment both with respect to $\tan\Psi$ and $\cos\Delta$. We note that the model curves in this case actually oscillate about the data, indicating that the model calculation is simulating to the best degree possible within its limitations a graded surface region.

By examining the sequence of increasingly better models in Fig. 5, it is apparent that the sample can be described as having a surface roughness of thickness of the order of 100 Å, with the top 50 Å containing essentially as much a-Si as voids. As will be discussed in Sec. IV D, this is not compatible with pyramid models, but fits rather a hemispherical bump distribution as expected from growth by nucleation. The layer here is too thin to investigate in more detail: attempts to minimize mean-square deviations with two layers resulted in negative thicknesses of the outer layer indicating that the accuracy limit of the data had been reached.

C. Rough sample

Similar results for the rough sample, whose TEM replica is shown in Fig. 1, are summarized in Fig. 7 and given in detail in Table III. For these computations, 66 points were used from 2.1 to 5.5 eV. Comparisons between measured and calculated $\tan\Psi$ and $\cos\Delta$ spectra are shown in Fig. 8 for the best two-parameter and the best overall fits. These have $\hat{\sigma}$ values of 0.089 and 0.021, respectively, and are therefore approximately equivalent to the two spectra chosen for Fig. 6.
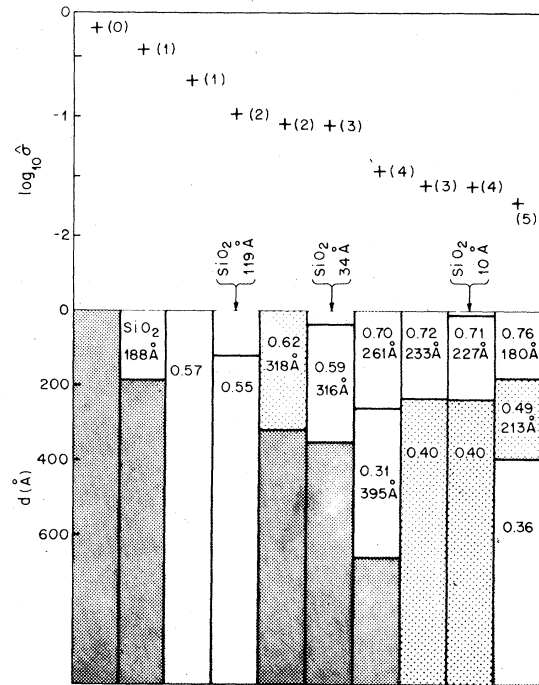

FIG. 7. As in Fig. 5, but for microscopically rough sample.

Figure 7 shows unambiguously that significantly better fits are obtained under equivalent restrictions (e.g., an a-Si substrate) by increasing the number of effective-medium overlayers. Further, the void fraction in multilayer solutions increases as the surface is approached. This correlates exactly with the expected

TABLE III. Best-fit parameters and their 90% confidence limits for the rough sample (see Fig. 7), listed in increasing goodness of fit.

| Substrate	First layer	Second layer	$\hat{\sigma}$
a-Si	$\cdots$	$\cdots$	0.55
a-Si	SiO_2, $d = 188 \pm 48$ Å	$\cdots$	0.37
a-Si + void $(57 \pm 3\%)$	$\cdots$	$\cdots$	0.20
a-Si + void $(55 \pm 2\%)$	SiO_2, $d = 119 \pm 14$ Å	$\cdots$	0.11
a-Si	a-Si + void $(62 \pm 2\%)$, $d = 318 \pm 15$ Å	$\cdots$	0.089
a-Si	a-Si + void $(59 \pm 2\%)$, $d = 316 \pm 16$ Å	SiO_2, $d = 34 \pm 19$ Å	0.086
a-Si	a-Si + void $(31 \pm 2\%)$, $d = 395 \pm 28$ Å	a-Si + void $(70 \pm 1\%)$, $d = 261 \pm 9$ Å	0.036
a-Si + void $(40 \pm 2\%)$	a-Si + void $(72 \pm 1\%)$, $d = 233 \pm 7$ Å	$\cdots$	~ 0.0272
a-Si + void $(40 \pm 2\%)$	a-Si + void $(71 \pm 2\%)$, $d = 277 \pm 11$ Å	SiO_2, $d = 10 \pm 11$ Å	0.0269
a-Si + void $(36 \pm 3\%)$	a-Si + void $(49 \pm 9\%)$, $d = 213 \pm 54$ Å	a-Si + void $(76 \pm 4\%)$, $d = 180 \pm 49$ Å	0.021
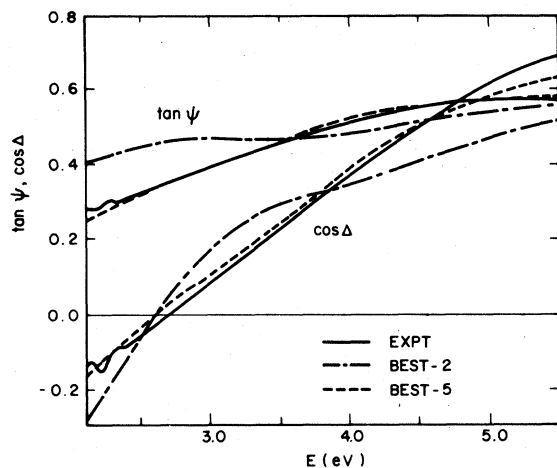
FIG. 8. As in Fig. 6, but for best two- and five-parameter fits for microscopically rough sample. Data (———) are compared to best two-parameter (— — — — -) and best overall (— — —) models of Fig. 7.

characteristics of a microscopically rough surface, as can also be seen from Fig. 1. To our knowledge, this is the first optical measurement that has demonstrated explicitly the existence of density gradients in the surface region of a microscopically rough material.

As with the moderately rough sample, it is clear that better representations of the rough sample are obtained by not using SiO_2 as the outer layer, and by assuming that the assumed infinite substrate is itself uniformly penetrated by a small fraction of voids. But by comparison to the moderately rough sample, the outer layers now have a very large fraction of voids. Is this an attempt by the model to simulate SiO_2? The answer is no: over the energy range 1.5–5.8 eV, the nearest EMA representation of SiO_2 formed by combining a-Si with voids occurs at a void concentration of 0.836, and the distinction between SiO_2 and its nearest EMA approximation is easily made above 3 eV (though not below) because of the relatively strong absorption of the latter in the near uv. Thus the lower surface density is a real material effect and not due to the presence of an anomalously thick oxide overlayer.

The requirement of voids in the substrate material is consistent with TEM micrographs and indicates further that the overall thickness of the roughness layer must be comparable to the penetration depth of the light. From the best-fit model of Fig. 7, the thickness of the two outer roughness layers is about 400 Å, which is reasonable in view of Fig. 1. Taking from Figs. 3 and 4 the mean values $\epsilon_2 \sim 5$, $\lambda = 3500$ Å, and $n \sim 2$, we find $\alpha^{-1} = n\lambda/2\pi\epsilon_2 \sim 220$ Å, in good agreement with the thickness of the optically absorbing intermediate layer in the best-fit model of

Fig. 7. Thus the light penetration depth fairly closely matches the overall thickness of the roughness layer near the spectrum center, which is probably near optimum for characterizing density distributions in microscopically rough surfaces. Although the penetration depth is greater at longer wavelengths, it is probably not possible to determine accurately profile data at levels deeper than 500 Å in this material. Therefore the substrate, which in fact will include the lower region of microscopic roughness, appears to have a uniform density of voids. We note that the apparent substrate void concentration of the moderately rough CVD sample in Fig. 5 is substantially less, as expected if the roughness layer is thinner and the grain size smaller.

The penetration depth argument also shows that the higher-energy measurements provide information primarily about the surface region of the rough layer, while longer wavelengths probe more deeply. In effect, by tuning the wavelength one can select the penetration depth. Thus wavelength-dependent measurements will always be more definitive than fixed-wavelength measurements. This principle is also applicable to other systems such as oxides on semiconductors.[31]

The 90% confidence levels in Table III show a characteristic decrease followed by an increase as the number of parameters is varied. At first, the model is too crude to fit well and the uncertainty is large because $\hat{\sigma}$ is large. As the number of parameters increases, they become less distinct in their effects, i.e., they become more correlated. Because the 90% confidence limit must include correlation effects, two highly correlated parameters will show a large uncertainty simply because they compensate each other. This occurs for example for the void density of the middle layer and the thickness of the outer layer in the best-fit five-parameter model in Table III. These two parameters have a surprisingly high calculated Pearson correlation coefficient of −0.994. Thus the effect of a small change in one upon $\hat{\sigma}$ can be compensated almost exactly by a small change in the other, and consequently their uncertainties become relatively large. The correlation between the void density of the *middle* layer and the thickness of the *outer* layer is not at all obvious and can only be discovered by statistical analysis. The statistical analysis also shows other features worth noting. The improvement gained by adding the SiO_2 layer in the next-best model in Table III is not statistically significant. Generally speaking, void concentrations in the substrate and all parameters of outer layers are determined most definitively from the data. A six-parameter fit would most likely fail to yield significant results, as inferred by the increase in uncertainty upon going from four to five parameters.

It is clear that a multiparameter analysis requires adequate data input to succeed. The importance of
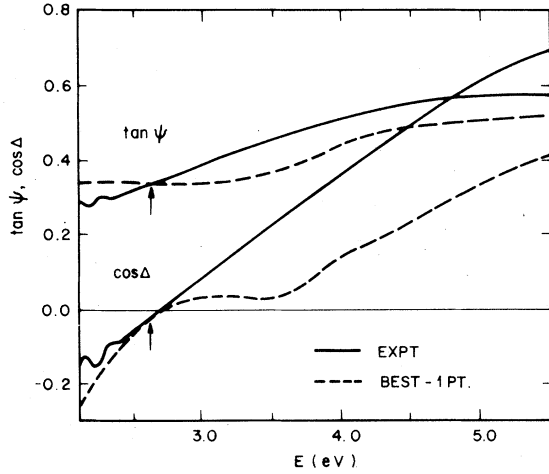
FIG. 9. As in Fig. 8, but best two-parameter model determined at a single point, 2.6 eV, indicated by the arrows.
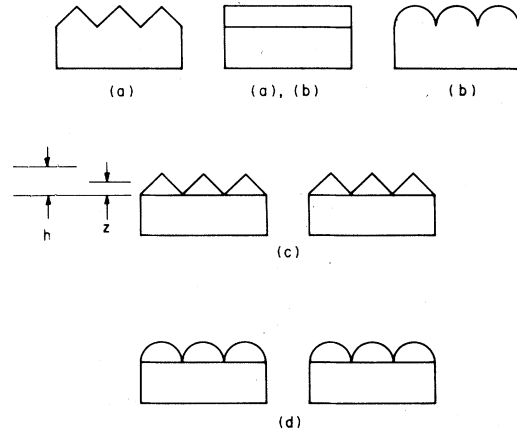

FIG. 10. Schematic diagram of roughness models used in the text. (a) Triangular ridges; (b) hemicylindrical ridges; (c) pyramids; and (d) hemicylindrical pyramids. The height parameters h and z are indicated for (c).

wavelength scanning to obtain adequate data can be appreciated from Fig. 9, which shows a comparison between $\tan\Psi$ and $\cos\Delta$ for the rough sample and a two-parameter model calculation that fits exactly at a single point, 2.6 eV. The energy of this point was chosen deliberately high compared to the energies normally attainable with null ellipsometers (5461 Å $= 2.270$ eV, 6328 Å $= 1.959$ eV) to reach a spectral region where the a-Si film was absorbing and the data therefore would not be distorted by back reflections from the substrate. Aside from that advantage, the spectra show that the one-point fit is unacceptable above 3 eV even though perfect at 2.6 eV. Thus a spectroscopic capability is essential.

D. Surface topography

Several rough-surface models involving ridges,[9,12,15] pyramids,[9,12,15] or similar geometric forms[2,3] have been used to stimulate surface roughness in computational models. In the absence of density profile data, however, it has not been possible previously to determine experimentally which geometric models may actually be appropriate. We shall use the best-fit results for the rough surface in Fig. 7 to show that a hemispherical model closely approximates our data. A hemispherical representation confirms film growth via a three-dimensional nucleation process.[37]

In accordance with the discussion in Sec. IV C, we shall assume that the rough-surface region penetrates about 150 Å beyond the 393 Å outer-layer thicknesses obtained in Fig. 7, and thus locate the plane dividing the rough-surface region from the substrate in the idealized model 550 Å below the surface. We obtain from Fig. 7 the density profile given in

Table III, recalling that the EMA and related theories deal with volume fractions thereby allowing us to compare geometric results directly with data.

We consider explicitly the four classes of shapes shown in Fig. 10. It is easy to show that the volume fraction of material lying between heights $0 \lesssim z_1/h \lesssim z_2/h \lesssim 1$ above the basal plane are given by: (a) triangular ridges

$$f_{21}^{tr} = 1 - (z_1 + z_2)/2h \; ; \tag{5a}$$

(b) hemicylindrical ridges

$$f_{21}^{hr} = \frac{(\theta_2 - \theta_1) + \frac{1}{2}(\sin2\theta_2 - \sin2\theta_1)}{2(z_2 - z_1)/h} \; ,$$

where

$$h\sin\theta_1 = z_1 \, , \quad h\sin\theta_2 = z_2 \; ; \tag{5b}$$

(c) pyramids

$$f_{21}^{p} = 1 - \frac{z_1 + z_2}{h} + \frac{z_1^2 + z_1 z_2 + z_2^2}{3h^2} \; ; \tag{5c}$$

(d) hemicylindrical pyramids

$$f_{21}^{hp} = 1 - \frac{z_1^2 + z_1 z_2 + z_2^2}{3h^2} \; . \tag{5d}$$

The latter two geometries imply complete filling of the basal plane area by the bases of the geometric figures. To convert them to close-packed cones or true hemispheres it is necessary to multiply the respective volume fractions by the ratio of the areas of the bases, that is, $\frac{1}{4}\pi$. Other geometries can be accommodated with different scaling factors.

Numerical values for five geometries are shown in Table IV. The numbers in parentheses are the calcu-

TABLE IV. Density profiles for various model rough surfaces compared to the best-fit model of Fig. 7. The values represent volume fractions of dielectric over the regions shown. Numbers in parentheses refer to basal areas scaled to give agreement with experiment for the bottom layer.

Model	0–180 Å	180–393 Å	393–550 Å
Data—Fig. 7	0.24 ± 0.02	0.51 ± 0.01	0.64 ± 0.01
(a) Triang. ridges	0.16(0.12)	0.52(0.39)	0.86(0.64)
(b) Hemi. ridges	0.51(0.33)	0.87(0.56)	0.99(0.64)
(c) Pyramids	0.04(0.03)	0.28(0.24)	0.74(0.64)
(d) Hemi. pyramids	0.29(0.19)	0.76(0.50)	0.97(0.64)
(e) Hemispheres	0.23(0.19)	0.60(0.50)	0.76(0.64)

lated volume fractions scaled to bring the bottom-layer density fraction in agreement with the experimental value. The 90% confidence levels shown are substantially less than those given in Table III because for a density analysis, we may fix the layer thicknesses and treat only the void fractions as adjustable parameters to avoid double-counting correlation effects. The best unscaled agreement occurs for hemispheres. After scaling, the hemicylindrical pyramids and hemispheres (which are indistinguishable in this model) provide the best agreement. The triangular ridge and pyramid models put far too little material into the topmost layer to explain the data. Thus we conclude that the rough layer can be modeled approximately by a hemispherical geometry, which is expected on the basis of three-dimensional nucleation growth.
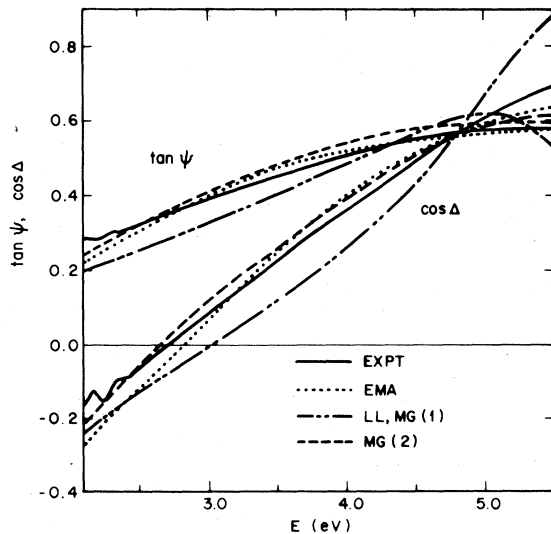

FIG. 11. Comparison of LL = MG(1), EMA, and MG(2) model calculations of tanΨ and cosΔ to experiment for the microscopic rough surface. A three-parameter configuration (see text) is used.

TABLE V. Best-fit parameters for three effective-medium models to the rough-surface data, as discussed in the text.

Model	v_{sub}	v_1	d_1 (Å)	$\hat{\sigma}$
LL = MG(1)	0.19	0.59	236	0.0757
EMA	0.41	0.72	233	0.0265
MG(2)	0.48	0.89	267	0.0286

E. Effective-medium models

The data have been analyzed within the EMA based on arguments given in Sec. III B. Our results, however, allow effective-medium models to be compared within a new context—that of describing microscopically rough surfaces. In this section we obtain best-fit parameters to the rough-surface data for the one-parameter models LL = MG(1), EMA, and MG(2), to investigate possible differences in the results. We use a three-parameter model consisting of a single layer of adjustable thickness, with both layer and substrate having void concentrations also treated as variable paramters. The five-parameter model shown in Fig. 7 was preferred, but the LL model would not converge to physically meaningful solutions beyond three parameters.

The results are shown in Fig. 11, and the parameters obtained to obtain these best fits are shown in Table V. The EMA yields the lowest value of $\hat{\sigma}$ as expected from bulk applications[47] because it treats material and void equally. The MG(2) model, which presumes voids to be inserted into the host material, is, however, nearly as good with respect to $\hat{\sigma}$. By inspection of Fig. 11, it is seen that the EMA and MG(2) models both fit the data equally well at low energies with the principal discrepancy appearing at high energies. This is reasonable, for as discussed with respect to light penetration the high-energy data emphasize the outer layer which is mostly voids and therefore best represented by LL = MG(1), where the medium is considered to be inserted in the void. Thus EMA values for the void concentrations of outer layers are preferred over the MG(2) values.

The LL model gives very poor agreement by comparison with either EMA or MG(2), being able to reproduce only qualitatively the spectral dependence of both tanΨ and cosΔ. This is not surprising on physical grounds because the major fraction of the rough layer is material, not voids. Figure 11, however, provides the first direct evidence that the LL model is a relatively poor approximation in rough-surface modeling despite its universal use.

*Exchange Scientist from Laboratoires d'Electronique et de Physique, 94450 Limeil-Brevannes, France.

[1]L. Tronstad, thesis (Trondheim, Norway, 1931) (unpublished).

[2]R. J. Archer, Nat. Bur. Stand. (U.S.) Misc. Publ. 256, 255 (1964).

[3]J. Kruger, Corrosion 22, 88 (1966).

[4]R. J. Lederich and J. J. Bellina, Jr., J. Opt. Soc. Am. 60, 1697 (1970).

[5]V. Brusic, M. G. Genshaw, and J. O'M. Bockris, Surf. Sci. 29, 653 (1972).

[6]J. P. Marton and E. C. Chan, J. Appl. Phys. 45, 5008 (1974).

[7]K. Vedam, Surf. Sci. 56, 221 (1976).

[8]T. Smith, Surf. Sci. 56, 252 (1976).

[9]K. Loschke and G. Kuhn, Krist. Tech. 11, 645 (1976).

[10]K. K. Svitashev, A. I. Semenenko, L. V. Semenenko, and N. L. Shvartz, Opt. Spektrosk. 43, 161 (1977) [Opt. Spectrosc. (USSR) 43, 88 (1977)].

[11]F. Hottier, R. Cadoret, and J. B. Theeten, in *Compte Rendue IV Colloque de Physique et Chimie des Surfaces Solides,* Vide, Suppl. 111 (1978).

[12]C. A. Fenstermaker and F. L. McCrackin, Surf. Sci. 16, 85 (1969).

[13]R. S. Sirohi, Opt. Commun. 1, 304 (1970); J. Phys. D 3, 1407 (1970).

[14]E. C. Chan and J. P. Marton, J. Appl. Phys. 45, 5004 (1974).

[15]R. M. Pashley, Surf. Sci. 71, 139 (1978).

[16]V. Bermudez, Opt. Commun. 23, 413 (1977).

[17]D. W. Berreman, J. Opt. Soc. Am. 60, 499 (1970).

[18]I. Ohlidal and F. Lukes, Opt. Acta 19, 817 (1972); Opt. Commun. 5, 323 (1972).

[19]I. Ohlidal, F. Lukes, and K. Navratil, Surf. Sci. 45, 91 (1974).

[20]R. M. A. Azzam and N. M. Bashara, *Ellipsometry and Polarized Light* (North-Holland, Amsterdam, 1977).

[21]M. D. Williams and D. E. Aspnes, Phys. Rev. Lett. 41, 1667 (1978).

[22]P. Beckmann, *The Depolarization of Electromagnetic Waves* (Golem, Boulder, 1968).

[23]D. V. Sivukhin, Zh. Eksp. Teor. Fiz. 21, 367 (1951).

[24]D. V. Sivukhin, Zh. Eskp. Teor. Fiz. 30, 374 (1956) [Sov. Phys. JETP 3, 269 (1956)].

[25]B. D. Cahan and R. F. Spanier, Surf. Sci. 16, 166 (1969).

[26]J. I. Treu, A. B. Callendar, and S. E. Schnatterly, Rev. Sci. Instrum. 44, 793 (1973).

[27]P. S. Hauge and F. H. Dill, IBM J. Res. Dev. 17, 472 (1973).

[28]D. E. Aspnes and A. A. Studna, Appl. Opt. 14, 220 (1975); in *Optical Polarimetry-Instrumentation and*

Applications, edited by R. M. A. Azzam and D. L. Coffeen (Society of Photo-Optical Instrumentation Engineers, Bellingham, Wash., 1977), Vol. 112, p. 62; Rev. Sci. Instrum. 49, 291 (1978).

[29]R. W. Stobie, B. Rao, and M. J. Dignam, J. Opt. Soc. Am. 65, 25 (1975); Appl. Opt. 14, 999 (1975).

[30]J. B. Theeten, R. P. H. Chang, D. E. Aspnes, and T. E. Adams (unpublished).

[31]D. E. Aspnes, J. B. Theeten, and R. P. H. Chang, J. Vac. Sci. Technol. (to be published).

[32]K. Nakamura, M. Kamoshida, A. Uehara, and R. Tatsumi, in *Laser-Solid Interactions and Laser Processing — 1978,* edited by S. D. Ferris *et al.,* AIP Conf. Proc. No. 50 (AIP, New York, 1979), p. 434.

[33]H. R. Philipp, J. Phys. Chem. Solids 32, 1935 (1971).

[34]D. T. Pierce and W. E. Spicer, Phys. Rev. B 5, 3017 (1972).

[35]T. I. Kamins, M. M. Mandurah, and K. C. Saraswat, J. Electrochem. Soc. 125, 927 (1978).

[36]N. Nagasima and W. Kubota, J. Appl. Phys. Jpn. 14, 1105 (1975).

[37]L. N. Alexandrov, F. L. Edelman, and V. V. Voskoboinikov, Vacuum 27, 145 (1977).

[38]J. Y. W. Seto, J. Electrochem. Soc. 122, 701 (1975).

[39]A. Marvin, R. Toigo, and V. Celli, Phys. Rev. B 11, 2777 (1975).

[40]D. E. Aspnes, J. Opt. Soc. Am. 64, 812 (1974).

[41]C. G. Grandqvist and O. Hunderi, Phys. Rev. B 16, 3513 (1977).

[42]R. Landauer, in *Proceedings of the First Conference on the Electrical Transport and Optical Properties of Inhomogeneous Media,* edited by J. C. Garland and D. B. Tanner, AIP Conf. Proc. No. 40 (AIP, New York, 1978).

[43]D. Stroud, Phys. Rev. B 12, 3368 (1975).

[44]J. C. Maxwell Garnett, Philos. Trans. R. Soc. London 203, 385 (1904); A205, 237 (1906).

[45]D. A. G. Bruggeman, Ann. Phys. (Leip.) 24, 636 (1935).

[46]Z. Hashin and S. Shtrikman, J. Appl. Phys. 33, 3125 (1962).

[47]R. Landauer, J. Appl. Phys. 23, 779 (1952).

[48]R. W. Cohen, G. D. Cody, M. D. Coutts, and B. Abeles, Phys. Rev. B 8, 3689 (1973).

[49]J. I. Gittleman and B. Abeles, Phys. Rev. B 15, 3273(1977).

[50]C. G. Grandqvist and O. Hunderi, Phys. Rev. B 18, 2897 (1978).

[51]C. Kühl, H. Schlötterer, and F. Schwidefsky, J. Electrochem. Soc. 121, 1496 (1974).

[52]*American Institute of Physics Handbook,* 3rd ed., edited by D. E. Gray (McGraw-Hill, New York, 1972), p. 6-29.

[53]E. S. Keeping, *Introduction to Statistical Inference* (Van Nostrand, Princeton, 1962), Chap. 12.
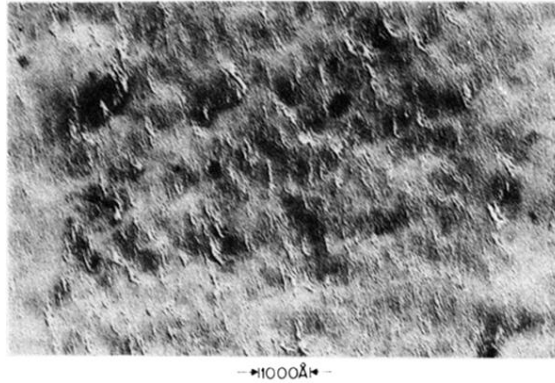
— ⊢1000Å⊢ —

FIG. 1. TEM micrograph of Pt-shadowed replica of the surface of the roughest sample investigated here. Magnification is indicated in figure.
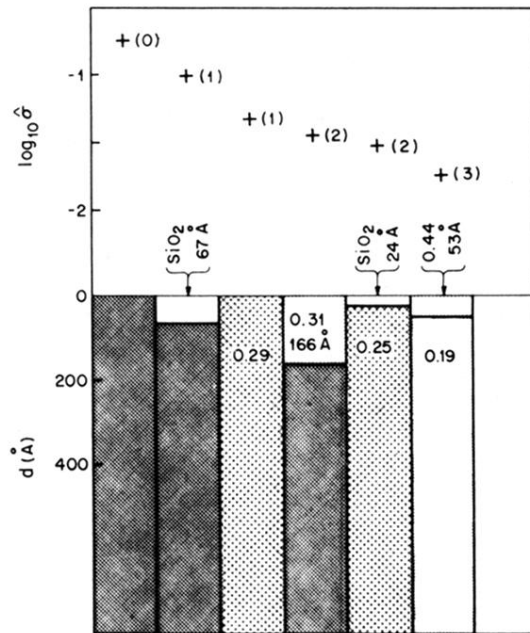
FIG. 5. Schematic of models of increasing complexity obtained by best-fit comparisons of calculated values of ρ to moderately-rough-sample data. Values of $\hat{\sigma}$ are plotted at top. Numbers in lower bars, if given, represent volume fraction of voids in a-Si as calculated in the EMA. Uncertainties are given in Table II.